SELECTING CAPILLARY STRUCTURES FOR HEAT PIPES IN MULTILAYER PRINTED CIRCUIT BOARDS

W.W. Wits[1], R. Legtenberg[2] and J.H. Mannak[2]
[1]University of Twente, Faculty of Engineering Technology, Enschede, The Netherlands
[2]Thales Nederland, Hengelo, The Netherlands

Abstract

Heat pipes are increasingly used to manage heat dissipations in electronic products. In a novel design approach for these products, a flat miniature heat pipe has been integrated inside the laminated structure of a printed circuit board (PCB). The capillary wick structure, required to facilitate the fluid transport, in combination with the orientation of the embedded heat pipe determines, to a large extent, the heat pipe's performance. Important design parameters are the wick's effective pore size and permeability, together with production and assembly requirements. A narrow pore gives great capillary pressure, however more friction is encountered. In general, as the gravitation assisted fluid flow decreases, so does the design freedom to select a type of wick. For gravity assisted orientations an open wick structure, such as microgrooves, channels and arteries, is preferred, whereas against gravity a more compact wick, for instance a sintered metal wick, is required. The optimal capillary structure should be selected for the intended application and production volume, thus obtaining sufficient heat transport, at the lowest manufacturing cost.

Nomenclature

		Subscripts			
α	aspect ratio	*ar*	artery	*sc*	screen
F	frictional coefficient	*ch*	channel	*sm*	sintered metal
f	friction factor	*eff*	effective	*st*	stub
K	permeability [m^2]	*gr*	groove	*t*	total
N	number of grooves	*h*	hydraulic	*w*	wick

1 Introduction

Thermal management plays an increasingly dominant role in the design process of electronic products. Component sizes decrease while performance demands increase, resulting in more power dissipation on smaller surfaces. In circuit card assemblies (CCAs), thermal management is hampered by the fact that their organic multilayer PCBs are generally poor thermal conductors and also by the common practice that thermal issues are usually addressed towards the end of the design process. As a result a wide variety of add-on cooling equipment (e.g. heat sinks, fans) is required to effectively manage the heat dissipation of electronic components mounted on the CCA. Due to the continuous miniaturization, the limits of these solutions are being reached (Lasance and Simons, 2005). Therefore, two-phase cooling solutions (e.g. heat pipes, vapour chambers), offering better thermal performance, are increasingly used in the design of electronic products. Regrettably, in most of these products no integrated design approach is incorporated: cooling remains to be add-on equipment.

The use of heat pipes as a reliable thermal management device for electronics cooling was first introduced by Cotter (1965). Cao et al. (1993) presented a comprehensive review of miniature heat pipes and their operating limitations. Jones et al. (2002) reported micro heat pipes embedded in

laminate substrates, based on a wick structure of microgrooves realized by stacking dielectric layers in a staggered lay-up. In this case, heat pipe failure occurred around 10W due to delamination of the PCB. In a previous publication of this study (Wits et al., 2006) a new heat pipe design was presented. A heat pipe was fully integrated into a CCA, using only standard PCB production and surface mount device (SMD) assembly techniques, as shown in Figure 1.

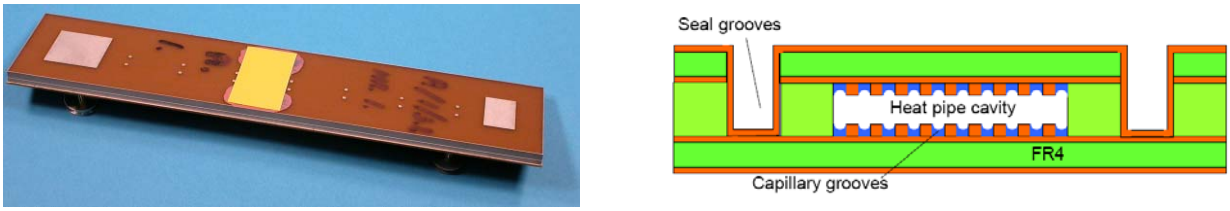

(a) technology demonstrator *(b) basic heat pipe structure*

Figure 1: *Heat pipe integrated into a circuit card assembly.*

This paper presents several designs for the mentioned integrated heat pipe. In practice, (high performance) electronic boards are mainly mounted either horizontally or vertically in a rack structure. Liquid rack cooling is common for these high performance boards. The challenge is to transport the heat effectively from the electronic components on the board, to the sides, where the board is clamped. Here, the heat can be dissipated through the rack structure to the ambient. As heat pipes are sensitive to their orientation, the design of the heat pipe embedded in the CCA depends on the way it will be installed. Special attention is given to the selection of the capillary structure inside the heat pipe. Different structures are illustrated and compared to each other.

2 Heat Pipe Design

Traditionally, a heat pipe is manufactured as a tubular metal structure. It encompasses three essential parts: an evaporator, an adiabatic transport zone and a condenser, as shown in Figure 2(a). A heat flux entering the evaporator vaporizes any available coolant liquid; this absorbs large quantities of heat. The vapour travels through the transport zone to the condenser, propelled by the difference in pressure. In the condenser the vapour condenses, releasing its latent heat. To complete the cycle the condensed liquid is transported back to the evaporator by means of a capillary wick structure. Selecting an optimal type of wick is subject of investigation in this paper.

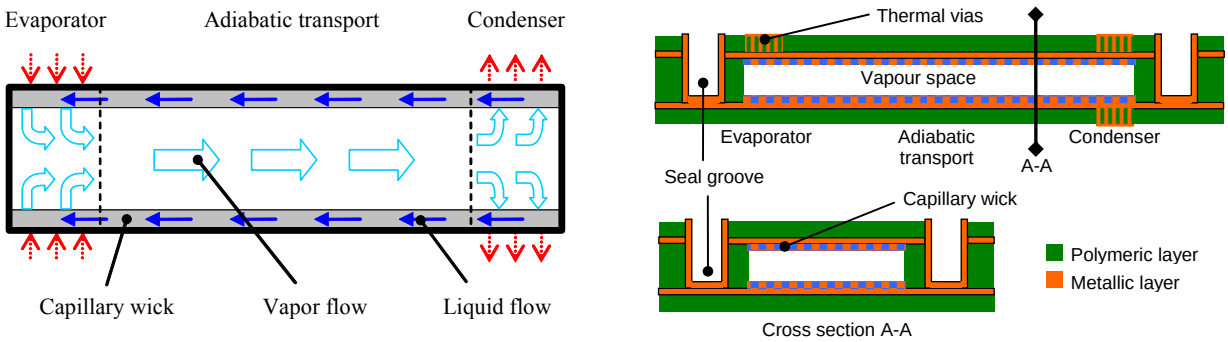

(a) traditional *(b) embedded in a multilayer PCB*

Figure 2: *Heat pipe design.*

In order to minimize cost, the heat pipes are manufactured using established PCB multilayer and surface mount assembly technology. A typical multilayer PCB consists of polymeric layers pressed together with bonding layers in between. On each polymeric layer a metallic pattern can be produced. This feature can be used to produce the wick structure, as will be shown in Section 2.1. The heat pipe vapour space is realized by machining a cavity in an intermediate layer. Figure 2(b)

illustrates an embedded heat pipe using one (thicker) intermediate layer. The height of the heat pipe can also be varied by stacking multiple layers in between the heat pipe's top and bottom layer. As the polymeric laminates and bonding layers are permeable to both water and gases, a copper plated groove is fabricated around the heat pipe cavity, ensuring a hermetically sealed enclosure. At the evaporator and condenser region, heat must travel through the laminated PCB layers. These polymeric layers are poor thermal conductors; hence to transfer heat into and out of the embedded heat pipe, an array of thermal vias is placed on both sides.

2.1 Wick Structure

To transport the working fluid from the condenser back to the evaporator, a wick structure is incorporated on the heat pipe's top and bottom layer. As transport is based on capillary effects, the effective radius of the structure should be small. This causes a higher (capillary) pressure difference across the heat pipe. However, the radius should not be too small, as this causes a low permeability of the wick due to frictional effects. In addition to this geometric feature, the heat pipe orientation is also important. Body forces acting on the liquid can either increase or diminish its flow. To maximize heat pipe potential, in general, an open wick structure is preferred in a gravity-assisted orientation. When the liquid has to ascend against gravity, a more compact wick is required.

In this paper the capillary effects, permeability and heat pipe orientation are investigated for five different types of wick, as listed in Table 1. In all cases the heat pipe's performance is evaluated by its ability to transport power from the evaporator to the condenser end.

Table 1: *Case of wick structure.*

I	Rectangular microgrooves
II	Supported foil channel
III	Wire screen
IV	Sintered metal
V	Screen covered artery

Rectangular microgrooves
Rectangular capillary microgrooves are positioned axially along the heat pipe length. A cross section of the basic design is illustrated in Figure 3(a). In operation, the liquid height at the evaporator side recedes due to the vaporization. As condensation occurs at the other end, there will be more liquid at the condenser side. Pressure difference to transport the liquid, is caused by the difference in meniscus and thus by the liquid height in the grooves, as illustrated by Figure 3(b). The maximum capillary pressure is determined by the width of the grooves.

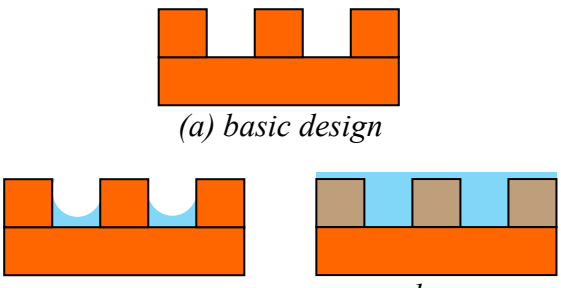

(a) basic design

(b) local liquid height

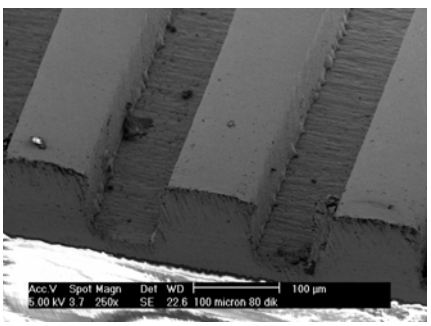

(c) produced on PCB laminate

Figure 3: *Rectangular microgrooves.*

Figure 3(c) shows a PCB laminate on which a microgroove structure is produced. It is realized by a selective plating process, common to PCB fabrication processes. Experiments indicated a minimum groove width of 50µm, based on conventional dry film lithography. Below this boundary, the resist stripping process used showed problems to effectively strip the resist from the microgrooves after plating. The smallest applied spacing (stubs) between grooves were 75µm. The permeability of these grooves is relatively high compared to, for instance, sintered porous structures. However, in counter-gravity orientations the liquid ascents poorly. Also the effect of the counter-flowing vapour across the liquid surface must be taken into account.

Supported foil channel

By laminating an additional copper foil into the CCA, a channel to transport the liquid can be realized. Figure 4(a) shows a single channel across the entire liquid cross section. Although sagging of the foil will not completely deteriorate heat pipe performance, it will be difficult to predict the actual cross section and thus required liquid volume to fill the heat pipe. This can be prevented by either plating or etching additional copper stubs, as shown in Figure 4(b). Depending on the number of stubs, multiple channels can be created and local support of the foil is realised.

(a) one channel *(b) multiple channels*

Figure 4: *Supported foil channel.*

At the evaporator and condenser end an opening in the foil has to be made, to allow the vapour and condensate to be exchanged. The maximum capillary force previously dominated by the width of the grooves, is now determined by the dimensions of the channel(s). In general, the radius will be smaller than for the microgrooves. However, the permeability generally has the same order of magnitude. As the channels are closed, there is no liquid-vapour interaction.

Wire screen & sintered metal

Instead of producing the wick using standard PCB processes, a wick manufactured separately can also be used. A wire screen or sintered metal wick can be placed inside the heat pipe cavity prior to laminating the CCA, as shown in Figures 5(a) and 5(b), respectively. The maximum capillary pressure is determined by the average pore size; generally this is better than grooved or channel structures. However, the permeability of these wicks is lower; therefore there will be more frictional losses. Both structures must be fixed onto the top or bottom layer of the heat pipe. To obtain a good thermal contact, pressure should be applied. This can be realized by, for instance, protrusions in either the porous structure or opposite layer.

(a) wire screen *(b) sintered metal* *(c) screen covered artery*

Figure 5: *Other wick structures.*

Screen covered artery

Through a composite wick both a low pore radius and high permeability can be obtained. The artery is produced using standard PCB processes, just as the grooves and channels. Prior to laminating the CCA, a screen in placed on top of the artery. This is illustrated in Figure 5(c). The artery acts as an open channel, whereas the screen supplies high capillary pressure.

2.2 Thermal Design

One of the pitfalls in integrated heat pipe design for CCAs is the thermal path at the evaporator and condenser end. As this does not influence steady state operation it is usually not included in heat pipe performance calculations. Heat should be transported efficiently to the actual evaporation and condensation sites. Traditional heat pipe geometries often have a proper thermal path, due to their metal form and tubular shape. In the case of an integrated heat pipe with a rectangular shape this is not the case. Although the thermal path for microgrooves, wire screen and sintered metal is acceptable, for the supported foil channel and screen covered artery this may cause unacceptable temperature gradients. Here most heat is conducted around the poorly conducting liquid, through the thin foil or screen, to the evaporation site, as illustrated in Figure 6(a). To optimize the thermal path, copper stubs, visible in Figure 6(b), can be added. This design is similar to the multiple channel wick, however in the adiabatic transport section these stubs are not necessary.

(a) normal *(b) with added copper stubs*

Figure 6: *Thermal path for a supported foil channel.*

3 Wick Performance

During operation, a heat pipe can encounter various limitations. In the application of electronics cooling the most critical limitation for flat miniature heat pipes is the capillary limit (Cao et al, 1993). This limit is reached when the wick structure cannot pump sufficient working fluid to the evaporator region. Therefore the wick's ability to transport liquid efficiently determines, to a great extend, the overall heat pipe performance. High permeability, low friction and no vapour-liquid interaction are preferred. The performance also depends on the heat pipe's orientation and operating temperature. Faghri (1995) and Cao et al. (1996) present some analytical expressions to describe the capillary limit. The maximum transferable power $Q_{cap,max}$ at this limit can be expressed as:

$$Q_{cap,\max} = \frac{\frac{2\sigma}{R_{eff}} + \rho_l g L_t \sin(\gamma)}{L_{eff}(F_l + F_g)} \tag{1}$$

where σ is the surface tension, R_{eff} the effective pore radius, L_t and L_{eff} the heat pipe's total and effective length respectively, γ the heat pipe's inclination angle and F the frictional coefficient. In this expression pressure losses due to phase changes and body forces on vapour particles are neglected. Also optimal wetting of the wick is assumed. In Equation (1) the effective pore radius of the wick structure depends on the type of wick. Table 2 lists the effective radius for each case. As evaporation and condensation, on average, occur halfway, the effective length of the heat pipe is expressed as:

$$L_{eff} = \tfrac{1}{2} L_{evaporator} + L_{adiabatic} + \tfrac{1}{2} L_{condenser} \tag{2}$$

The liquid and vapour frictional coefficients in Equation (1) are defined as, respectively:

$$F_l = \frac{\mu_l}{\rho_l A_w K_w h_{\lg}} \tag{3}$$

$$F_g = \frac{2\mu_g (f \operatorname{Re}_{g,h})}{\rho_g A_g D_{g,h}^2 h_{\lg}} \tag{4}$$

where μ is the dynamic viscosity, K_w the permeability of the wick structure, h_{lg} the latent heat of vaporization and *fRe* the Reynolds friction factor. In these expressions the hydraulic diameter and hydraulic Reynolds number are used, as both cross sections have rectangular geometries. The liquid hydraulic diameter depends on the type of wick. Permeability, hydraulic diameter and porosity φ, as shown in Table 2, are also adopted from Faghri (1995).

Table 2: *Wick properties.*

Case	R_{eff} [m]	K_w [m^2]	$D_{l,h}$ [m]	φ [-]
I. Rectangular microgrooves	W_{gr}	$\frac{D_{l,h}^2\varphi}{2(f\,\mathrm{Re}_{l,h})}$	$4\frac{W_{gr}\cdot H_{gr}}{W_{gr}+2H_{gr}}$	$\frac{W_{gr}}{W_{gr}+W_{st}}$
II. Supported foil channel	$\frac{W_{ch}\cdot H_{ch}}{W_{ch}+H_{ch}}$	$\frac{D_{l,h}^2}{2(f\,\mathrm{Re}_{l,h})}$	$2\frac{W_{ch}\cdot H_{ch}}{W_{ch}+H_{ch}}$	
III. Wire screen	$\frac{W_{sc}+D_{sc}}{2}$	$\frac{D_{sc}^2\varphi^3}{122(1-\varphi)^2}$		$\approx 1-\frac{1.05\pi D_{sc}}{2R_{eff}}$
IV. Sintered metal	$0.21D_{sm}$	$\frac{D_{sm}^2\varphi^3}{150(1-\varphi)^2}$		≈ 0.40
V. Screen covered artery	$\frac{W_{sc}+D_{sc}}{2}$	$\frac{D_{l,h}^2\varphi}{2(f\,\mathrm{Re}_{l,h})}$	$4\frac{W_{ar}\cdot H_{ar}}{W_{ar}+2H_{ar}}$	$\frac{W_{ar}}{W_{ar}+W_{st}}$

Here, the width W, height H and diameter D are geometrical features of the wick. In the case of a screen the width W_{sc} equals the distance between the wires. D_{sm} is the diameter of the spherical metal particles used to fabricate the sintered wick. For all wick structure cases, the vapour hydraulic diameter is the same and equals:

$$D_{g,h} = 2\frac{H_g W_g}{H_g + W_g} \tag{5}$$

To compute the vapour velocity its friction factor must be estimated. Even if the vapour is in contact with the counter-flowing liquid, the liquid velocity is low compared to the vapour velocity. Therefore, the liquid velocity is negligible at the liquid-vapour interface. According to Shah and Bhatti (1987) the vapour friction factor $fRe_{g,h}$ can be expressed as:

$$f\,\mathrm{Re}_{g,h} = 24\left(1-1.3553\alpha+1.9467\alpha^2-1.7012\alpha^3+0.9564\alpha^4-0.2537\alpha^5\right) \tag{6}$$

where α represents the aspect ratio of the vapour flow cross section: H_g/W_g (or W_g/H_g if $H_g > W_g$).

To compute the liquid velocity its friction factor must also be estimated. In the case of the capillary microgrooves the shear stress at the liquid-vapour interface must be taken into account. Schneider and DeVos (1980) considered the effect of a planar free liquid surface in their expressions:

$$f\,\mathrm{Re}_{l,h} = (f\,\mathrm{Re}_{l,h})_0\left(1+\frac{N_{gr}W_{gr}^3}{6\pi D_{g,h}^3}(f\,\mathrm{Re}_{g,h})\frac{\upsilon_g}{\upsilon_l}\left[1-1.971e^{\frac{-\pi H_{gr}}{W_{gr}}}\right]\right) \tag{7}$$

$$(f\,\mathrm{Re}_{l,h})_0 = 8H_{gr}^2\left[\left(H_{gr}+\frac{W_{gr}}{2}\right)^2\left(\frac{1}{3}-\frac{32W_{gr}}{\pi^5 H_{gr}}\tanh\frac{\pi H_{gr}}{W_{gr}}\right)\right]^{-1} \tag{8}$$

where N_{gr} is the number of microgrooves and v the kinematic viscosity. In the case of the supported foil channel, liquid-vapour interaction is not possible, as the liquid flows through a closed cavity. Therefore, Equation (6) can be used to calculate the liquid friction factor as well. As through the screen of the covered artery interaction is possible, Equations (7) and (8) should be used.

4 Numerical Simulations

To select an optimal capillary structure for the embedded heat pipe, each case is evaluated numerically. As the heat pipe is embedded in a CCA, height is a restrictive parameter. The total height of the multilayer PCB should be a thin as possible. Figure 7 shows the heat pipe performance for increasing orientation angles. The counter-gravity orientation, i.e. evaporator placed above the condenser, is indicated by -90°, horizontal orientation is 0° and the gravity assisted orientation has an angle of +90°. In Figure 7(a) the height of each wick structure is 100µm, in Figure 7(b) this is increased to 200µm. In the case of microgrooves an aspect ratio of unity is observed; channels have a fixed width of 400µm. Effective pore radius and permeability values for the sintered metal are adopted from Mwaba et al. (2006): 30µm and $1.17 \cdot 10^{-11} m^2$, respectively. The screen is a 150-mesh screen which has a wire diameter of 25µm and a width between wires of about 144µm.

The heat pipe's total width and vapour space dimensions are equal for all cases. Based on the average footprint of a high power component, the width is 20mm. The height of the vapour space is 2mm; lower values dramatically increase friction effect on the vapour flow. As our design is used for electronics cooling, a constant internal temperature of 70°C is assumed for all cases. Please note the scaling on the Y-axis of both figures. In practice, a negative power value is not possible; however to gain more insight they are shown.

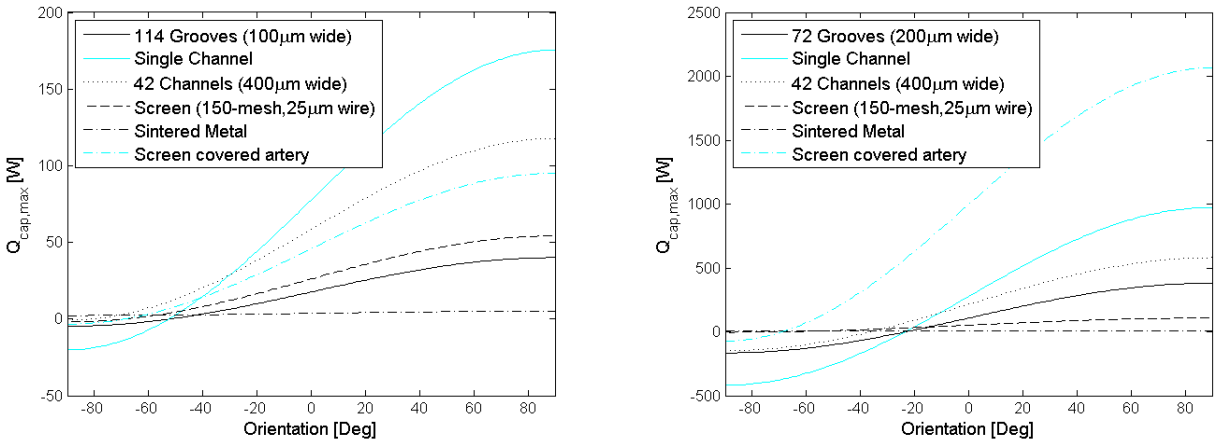

(a) 100µm wick height *(b) 200µm wick height*

Figure 7: *Heat pipe performance vs. orientation angle.*

As expected, for all cases performance increases as the heat pipe is tilted towards a more gravity assisted orientation. For all wicks, similar S-shaped trends are obtained, although for the sintered metal wick this effect is very small (and therefore not well visible). As wick sizes double, the maximum transportable power, both negative and positive values, amplifies. In all cases, except for sintered metal, heat transport is not possible when the liquid has to ascent straight up against gravity. Figure 7 also shows that open wick structures and a wire screen are very sensitive to the inclination angle. For the sintered metal wick the orientation is hardly relevant. The capillary and frictional components of Equation (1) outweigh the gravitational one. In this case, a double wick size, approximately doubles the heat pipe performance.

In general, in the gravity assisted orientation open wick structures perform better, as a compact wick hinders the flow of liquid. Horizontally, a composite or (multiple) channel wick shows promising results; liquid is supplied at lower frictional cost and the smaller effective radius improves the capillary pumping capability. Straight up against gravity only the sintered metal wick gives a positive performance.

5 Conclusions

Important design parameters to select an optimal capillary structure for heat pipes integrated in CCAs have been presented. Depending on the heat pipe's orientation different capillary structures are preferred. In gravity assisted orientations open wick structures, i.e. microgrooves, channels and arteries, show relative high performance values (> 40W), therefore one can select a type of wick that fits best with the production and assembly methods used and production volume demanded. Horizontally, a composite or (multiple) channel wick can transport relative large amounts of heat, especially for thin wick structures. If a robust design for any orientation is demanded, the sintered metal wick gives the best performance and should therefore be selected. Microgrooves and channel structures can be manufactured using established PCB production techniques. Wire screen and sintered metal wick structures must be manufactured separately; they are assembled during the lamination phase. The wick's thermal path should be observed, especially in case of open channel(s) and arteries.

Wick structures, in terms of heat capacity, wick size and type, and manufacturability can now be compared. Full integration of thermal management functions in electronic products pushes the boundary further towards more functionality and performance in a smaller form factor. Altogether, this can lead to more integrated electronic products, without protruding add-on cooling devices.

Acknowledgments

This work is part of the PACMAN project which is supported by the Netherlands Ministry of Economic Affairs, SenterNovem project number TSIT3049. The authors especially want to thank Pieter Nieboer and Bob Rots for their help on the heat pipe numerical simulations. We also thank the PCB production department of Thales Nederland for their support in evaluating different wick structures and possible lamination schemes.

References

Cao, Y., Faghri, A. and Mahefkey, T., 1993, Micro/Miniature Heat Pipes and Operating Limitations, ASME HTD-Vol. 236, pp. 55-62

Cao, Y., Gao, M., Beam, J.E. and Donovan, B., 1996, Experiments and Analyses of Flat Miniature Heat Pipes, Proc. IEEE Energy Conversion Engineering Conference (IECEC), Washington DC, USA, Vol. 2, pp. 1402-1409.

Cotter, T.P., 1965, Theory of Heat Pipes, Los Alamos Scientific Laboratory Report No. LA-3246-MS.

Faghri, A., 1995, Heat Pipe Science and Technology, Taylor & Francis, New York, USA.

Jones, K., Cao, Y. and Gao, M., 2002, Development of Micro Heat Pipes Embedded in Laminate Substrates for Enhanced Thermal Management for Printed Wiring Boards, Report Florida International University, Miami, USA.

Lasance, C.J.M. and Simons, R.E., 2005, Advances in high-performance cooling for electronics, ElectronicsCooling, Volume 11, Number 4.

Mwaba, M.G., Huang, X., Gu, J., 2006, Influence of wick characteristics on heat pipe performance, International Journal of Energy Research, Vol. 30, pp. 489-499

Schneider, G.E. and DeVos, R., 1980, Nondimensional Analysis for the Heat Transport Capability of Axially-Grooved Heat Pipes Inclusing Liquid/Vapor Interaction, AIAA Paper No. 80-0214.

Shah, R.K. and Bhatti, M.S., 1987, Laminar Convective Heat Transfer in Ducts, Handbook of Single-Phase Convective Heat Transfer, New York.

Wits, W.W., Legtenberg, R., Mannak, J. and Zalk, B. van, 2006, Thermal Management through In-Board Heat Pipes Manufactured using Printed Circuit Board Multilayer Technology, Proc. International Electronic Manufacturing Technology (IEMT), Putrajaya, Malaysia, pp. 55-61.